Available online at www.sciencedirect.com

SciVerse ScienceDirect

Ceramics International 38 (2012) 6411–6416

CERAMICS INTERNATIONAL

www.elsevier.com/locate/ceramint

Room temperature in situ chemical synthesis of Fe_3O_4/graphene

P.S. Teo[a], H.N. Lim[b,*], N.M. Huang[a], C.H. Chia[c], I. Harrison[d]

[a]*Low Dimensional Materials Research Centre, Department of Physics, Faculty of Science, University of Malaya, 50603 Kuala Lumpur, Malaysia*
[b]*Department of Chemistry, Faculty of Science, Universiti Putra Malaysia, 43400 UPM Serdang, Selangor, Malaysia*
[c]*School of Applied Physics, Faculty of Science and Technology, Universiti Kebangsaan Malaysia, 43600 Bangi, Selangor, Malaysia*
[d]*School of Chemical and Environmental Engineering, Faculty of Engineering, The University of Nottingham Malaysia Campus, Jalan Broga, 43500 Semenyih, Selangor, Malaysia*

Received 19 March 2012; received in revised form 4 May 2012; accepted 5 May 2012
Available online 26 May 2012

Abstract

A simple, cost-effective, efficient, and green approach to synthesize iron oxide/graphene (Fe_3O_4/rGO) nanocomposite using in situ deposition of Fe_3O_4 nanoparticles on reduced graphene oxide (rGO) sheets is reported. In the redox reaction, the oxidation state of iron(II) is increased to iron(III) while the graphene oxide (GO) is reduced to rGO. The GO peak is not observed in the X-ray diffraction (XRD) pattern of the nanocomposite, thus providing evidence for the reduction of the GO. The XRD spectra do have peaks that can be attributed to cubic Fe_3O_4. The field emission scanning electron microscopy (FESEM) images show Fe_3O_4 nanoparticles uniformly decorating rGO sheets. At a low concentration of Fe^{2+}, there is a significant increase in the intensity of the FESEM images of the resulting rGO sheets. Elemental mapping using energy dispersive X-ray (EDX) analysis shows that these areas have a significant Fe concentration, but no morphological structure could be identified in the image. When the concentration of Fe^{2+} is increased, the Fe_3O_4 nanoparticles are formed on the rGO sheets. Separation of the Fe_3O_4/rGO nanocomposite from the solution could be achieved by applying an external magnetic field, thus demonstrating the magnetic properties of the nanocomposite. The Fe_3O_4 particle size, magnetic properties, and dispersibility of the nanocomposite could be altered by adjusting the weight ratio of GO to Fe^{2+} in the starting material.

Keywords: B. Nanocomposite; Graphene; Iron oxide; Magnetite

1. Introduction

Graphene is a one-atom-thick two-dimensional (2D) single layer of sp^2-bonded carbon atoms arranged in a honeycomb lattice. It has a large active surface area, as well as unique electrical, thermal, and structural properties, and consequently it has many potential applications [1–4] (e.g., energy storage devices [5–8], drug delivery systems [9], waste water treatment [10–13], and sensing platforms [14–17]). A drawback of graphene is its poor dispersibility in solvents [18–20]. On the other hand graphene oxide (GO), with its abundance of oxygen-containing functional groups such as hydroxyl, epoxy and carboxyl groups, can be dispersed in either water or polar organic solvents and is a suitable substituent for graphene.

Low-cost magnetic iron oxides (magnetite Fe_3O_4 or maghemite *gamma*-Fe_2O_3) nanoparticles exhibit superparamagnetic nature, have low toxicity, and hence are biocompatible. However, heavy aggregation of the nanoparticles may limit their magnetic properties and structural stability, thus reducing their applicability. By creating a Fe_3O_4/graphene nanocomposite, the clumping of the Fe_3O_4 nanoparticles is reduced, preserving their unique properties.

Various methods of deposition of Fe_3O_4 nanoparticles on reduced graphene oxide (rGO) have been investigated (in situ formation [21], solvothermal method [22,23], hydrothermal method [24], covalent bonding method [25], and electrochemical method [26]). Depending on the fabrication method, the average size of Fe_3O_4 nanoparticles produced was in the range of 2 nm to 100 nm.

*Corresponding author. Tel.: +60163301609.
E-mail addresses: janet_limhn@yahoo.com, janet_limhn@science.upm.edu.my (H.N. Lim).

0272-8842/$36.00
http://dx.doi.org/10.1016/j.ceramint.2012.05.014

In this work, a simple, one-step, green, and efficient approach to the in situ chemical synthesis of iron oxide/graphene (Fe_3O_4/rGO) nanocomposite is reported. Since the synthesis is accomplished using a one-step reaction, the possibility of contamination of the Fe_3O_4/rGO composite produced is reduced. The one-step approach can also prevent the aggregation of reduced graphene sheets [27]. The synthesis method reported requires no toxic solvents and hence it is green and can be easily controlled by varying the process parameters. Moreover, the formation of Fe_3O_4/rGO nanocomposite occurs at room temperature, in contrast to other reported methods such as hydrothermal and chemical co-precipitation techniques which require high temperature. Thus the energy consumption is reduced compared to the alternatives, making the reported process cost-effective and green. The size of the particles in the nanocomposites could be modified by varying the weight ratio of graphene oxide (GO) and iron(II) ions (Fe^{2+}) in the starting material, allowing the modification of the properties of the nanocomposites to be optimized for various industrial and biotechnological applications.

2. Experimental

2.1. Materials

Graphite flakes were purchased from Ashbury Inc. Sulfuric acid (H_2SO_4, 98%), potassium permanganate ($KMnO_4$, 99.9%), hydrogen peroxide (H_2O_2, 30%), iron(II) sulphate ($FeSO_4.7H_2O$, 99.5%), and ammonium hydroxide (NH_4OH, 25%) were purchased from Systerm.

2.2. Preparation of graphene oxide

Graphite oxide was synthesized by oxidation of 3 g of graphite flakes with 400 ml of H_2SO_4 and 18 g of $KMnO_4$ (simplified Hummers' method [28]). The physical mixing of these chemicals, using a magnetic stirrer, took less than 5 min to complete. However, to ensure complete oxidation of the graphite, the mixture was stirred for 3 days. During the oxidation, the colour of the mixture changed from dark purplish green to dark brown. To stop the oxidation process, H_2O_2 solution was added and the colour of the mixture changed to bright yellow, indicating a high degree of oxidation of graphite. The graphite oxide formed was washed three times with 1 M of HCl aqueous solution and repeatedly with deionized water until a pH of 4–5 was achieved. The washing process was carried out by a simple decantation of the supernatant using a centrifugation technique. During the washing process with deionized water, the graphite oxide experienced exfoliation, which resulted in thickening of the GO solution, forming a GO gel which was subsequently freeze-dried to obtain the GO solid.

2.3. Preparation of Fe_3O_4/ rGO

The synthesis route of the Fe_3O_4/rGO nanocomposite is similar to a method previously reported [29]. The GO was dispersed in deionized water (DI) by stirring and underwent sonication for 20 min, which is essential to obtain a well dispersed solution. Then, 25% NH_4OH solution was added dropwise to the GO solution until the pH reached 11 or 12. The $FeSO_4$ solution was later added slowly to the GO solution under magnetic stirring and left overnight at room temperature. The next day, the black solution was centrifuged and washed three times with DI water for 10 min at 4000 rpm to remove the extra ammonium and then dried in vacuum. In the absence of GO, the Fe_3O_4 nanoparticles were obtained via the same process. Similarly, rGO was prepared using the same process without the presence of $FeSO_4$. The weight ratios between the GO and $FeSO_4$ are shown in Table 1. For all samples manufactured, the weight of GO in the starting material was held constant at 25 mg.

Table 1
Weight ratios between GO and $FeSO_4$ for the preparation of Fe_3O_4/rGO using in situ chemical synthesis method.

Sample	GO (mg)	$FeSO_4$ (mg)	Ratio (GO: $FeSO_4$)
G1F2	25	50	1:2
G1F5	25	125	1:5
G1F10	25	250	1:10
G1F20	25	500	1:20
G1	25	–	–
F20	–	500	–

2.4. Characterization

The crystalline phase was determined using a PANalytical Empyrean XRD employing a scanning rate of 0.033 $^{\circ}s^{-1}$ in a 2θ range from 5° to 70° with Cu-K_α radiation ($\lambda = 1.5418$ Å). Electron micrographs were obtained using an FEI Nova NanoSEM 400 FESEM.

3. Results and discussion

Due to the lack of surface functional moieties of the rGO, the sheets tend to aggregate and do not disperse in most solvents. However, the as-synthesized nanocomposites could be dispersed by sonication in polar solvents [27] such as water and ethanol, preventing the aggregation of rGO sheets and thus demonstrating the enhanced dispersibility in the polar solvents.

The magnetic properties of the nanocomposites were investigated by placing a permanent magnet next to the sample bottle. As expected, the F20 sample, containing only iron oxide particles without any solvent, moved under the external magnetic field to the side of the sample bottle (Fig. 1a). In the case of sample G1F2, the nanocomposite was well dispersed in an aqueous solution and remained unaffected by the external magnetic field (Fig. 1b). In contrast, the nanocomposite of G1F20 was attracted to the side of the sample bottle, leaving behind the transparent solvent. This occurred for both water (Fig. 1c) and ethanol

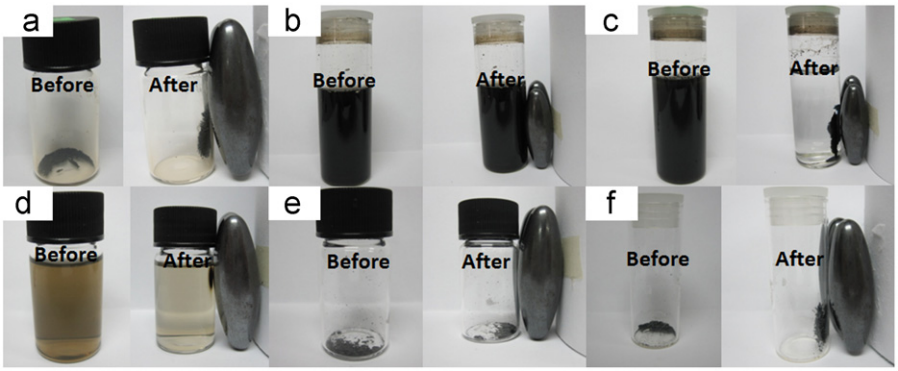

Fig. 1. Magnetic property and dispersibility of the samples: (a) powder F20, (b) dispersed G1F2 unaffected by the magnetic attraction, (c) G1F20 in water, (d) G1F20 in ethanol, (e) powder G1F2, and (f) powder G1F20.

(Fig. 1d). G1F5 and G2F10 also experienced the same magnetic attraction as G1F20 (images not shown). This result demonstrates the influence of the weight ratios of GO and Fe^{2+} on the magnetic behaviour of the nanocomposites. When the Fe^{2+}/GO weight ratio was increased, the separation of the nanocomposite from the solution occurred more quickly, suggesting an increase in the magnetic properties of the nanocomposites.

As expected, in the dry state, the G1F2 nanocomposite (Fig. 1e) failed to be attracted by the external magnetic field in comparison to the sample with a higher concentration of Fe^{2+} precursor (G1F20, Fig. 1f). The rate of attraction of the nanocomposites in the dry state also increased with the Fe^{2+} concentration in the starting material.

The structural information for G1, F20, and the nanocomposites is shown in Fig. 2. The sharp peak in the G1 XRD spectrum at $2\theta = 10.8^\circ$ corresponds to the (0 0 1) reflection of GO (Fig. 2a), indicating that GO was not completely reduced to rGO. However, for samples containing Fe^{2+} ions, apart from G1F2, this XRD line was absent, suggesting that the Fe^{2+} acts as a reducing agent for GO in the fabrication of the nanocomposites. In Fig. 2b, the series of diffraction peaks at $2\theta = 30.2^\circ$, 35.6°, 43.3°, 53.7°, 57.3°, and 62.8° is assigned to reflections from the (2 2 0), (3 1 1), (4 0 0), (4 2 2), (5 1 1), and (4 4 0) crystal planes of Fe_3O_4 (JCPDS no. 19–0629). These reflections and the absence of other impurity peaks suggest that the Fe_3O_4 nanoparticles are of good crystallinity. The XRD pattern of G1F2 has a sharp peak at $2\theta = 10.8^\circ$which corresponds to the (0 0 1) reflection characteristics of GO, while the diffraction peaks corresponding to Fe_3O_4 were not detected (Fig. 2c). The low content of Fe^{2+} ions in the starting material resulted in the incomplete reduction of GO. The low diffraction peak between 20° and 25° indicates a small degree of restacking of graphitic sheets [30]. We suggest that Fe_3O_4 formed on the surface of the partially reduced GO sheets, based on the ability of the nanocomposite to disperse homogeneously in an aqueous solution (Fig. 1b), in contrast to the rGO, which aggregates in most solvents, and the faint signature in the XRD

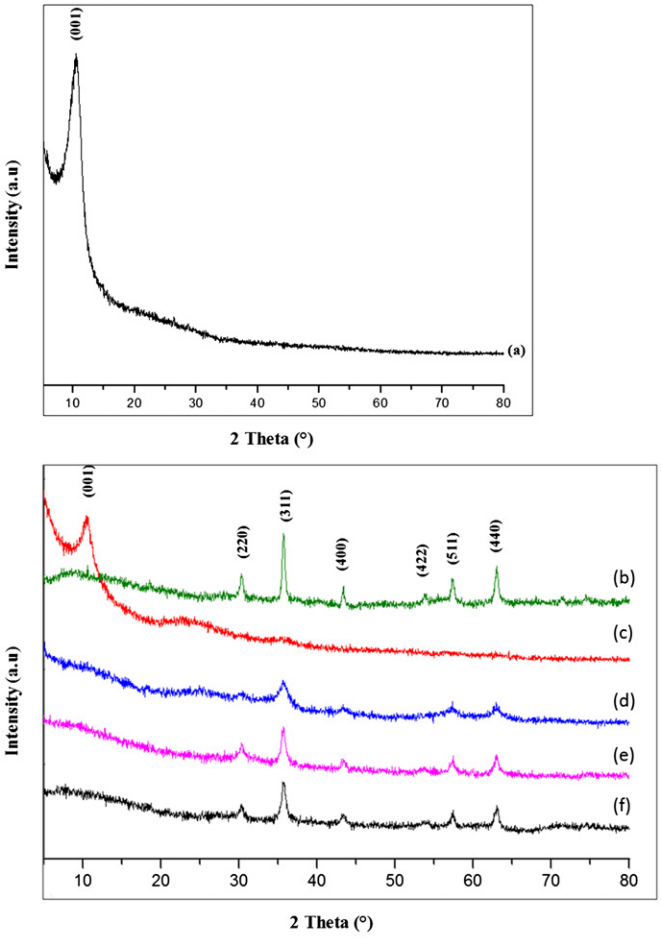

Fig. 2. XRD patterns of (a) G1, (b) F20, (c) G1F2, (d) G1F5, (e) G1F10, and (f) G1F20.

spectra at 35.6° which corresponds to reflections from the (3 1 1) planes of Fe_3O_4. When the concentration of Fe^{2+} was increased, five typical reflection peaks of Fe_3O_4 (30.2°, 35.6°, 43.3°, 57.3°, and 62.8°) were observed for G1F5, G1F10, and G1F20 (Figs. 2d–f). Furthermore, there is an inverse correlation between the width of the diffraction

peaks and the concentration of Fe^{2+}, indicating the smaller crystallite size of Fe_3O_4 in the nanocomposites synthesized using low Fe^{2+} concentrations. This result coincides with the observation from FESEM (Fig. 3). The graphitic peak for G1F5, G1F10, and G1F20 is missing because the attached nanoparticles hinder the formation of van der Waals and π–π stacking interactions between the rGO sheets [31].

Fig. 3 portrays the FESEM images of G1, F20, and the nanocomposites. G1 has a smooth surface with a distinctive layered appearance (Fig. 3a). F20, consisting of Fe_3O_4 nanoparticles, tends to agglomerate and has a wide distribution of particle sizes in the range of 50 nm to 250 nm (Fig. 3b). On the other hand, Fe_3O_4 nanoparticles are uniformly embedded on the surface of rGO sheets with a narrow size distribution for all the nanocomposites. The particle size of Fe_3O_4 nanoparticles steadily increased with increasing concentration of the $FeSO_4$ salt solution. The average particle sizes of G1F5 (Fig. 3d), G1F10 (Fig. 3e), and G1F20 (Fig. 3f) are 20 nm, 30 nm and 40 nm, respectively. There is no clear evidence for the formation of Fe_3O_4 nanoparticles in the FESEM image of G1F2 but there is contrast variation across the FESEM image. To investigate this further, elemental mapping of C, O, and Fe using energy dispersive X-ray (EDX) analysis (Fig. 3g) was undertaken (Fig. 3h). The area of bright contrast correlates with the Fe signal map. This result, coupled with the XRD result, provides evidence for the presence of Fe_3O_4 on the surface of the rGO. The exact form of the Fe_3O_4 cannot be determined. It is possible that a layer of Fe_3O_4 has formed on the surface of the rGO or more likely that very small nanoparticles have formed.

The synthesis of the Fe_3O_4/rGO nanocomposite involves the redox reaction between GO and Fe^{2+}. The schematic

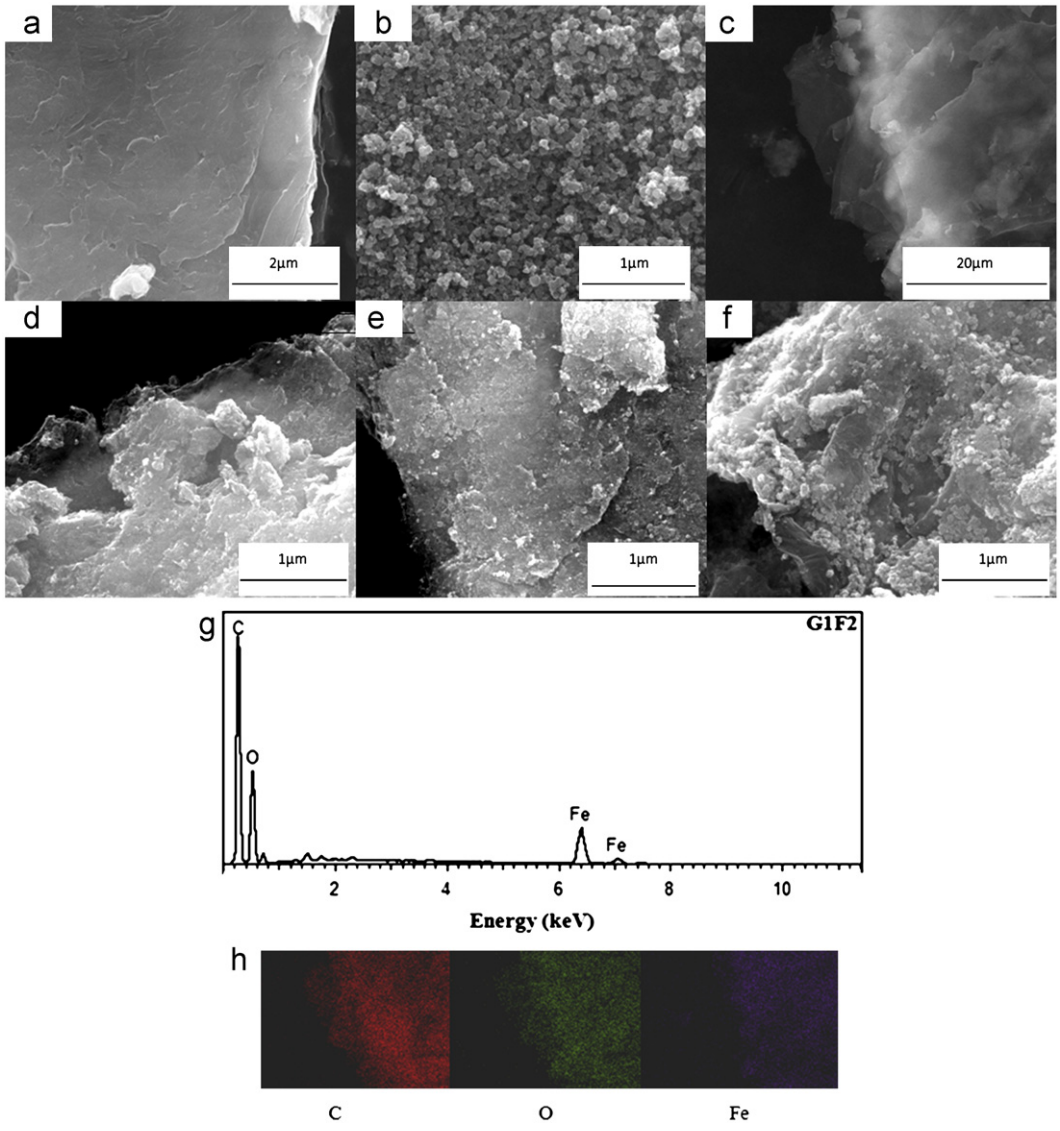

Fig. 3. FESEM images of (a) G1, (b) F20, (c) G1F2, (d) G1F5, (e) G1F10, and (f) G1F20; (g) EDX spectrum of G1F2; and (h) elemental mapping of G1F2 based on the image shown in (c).

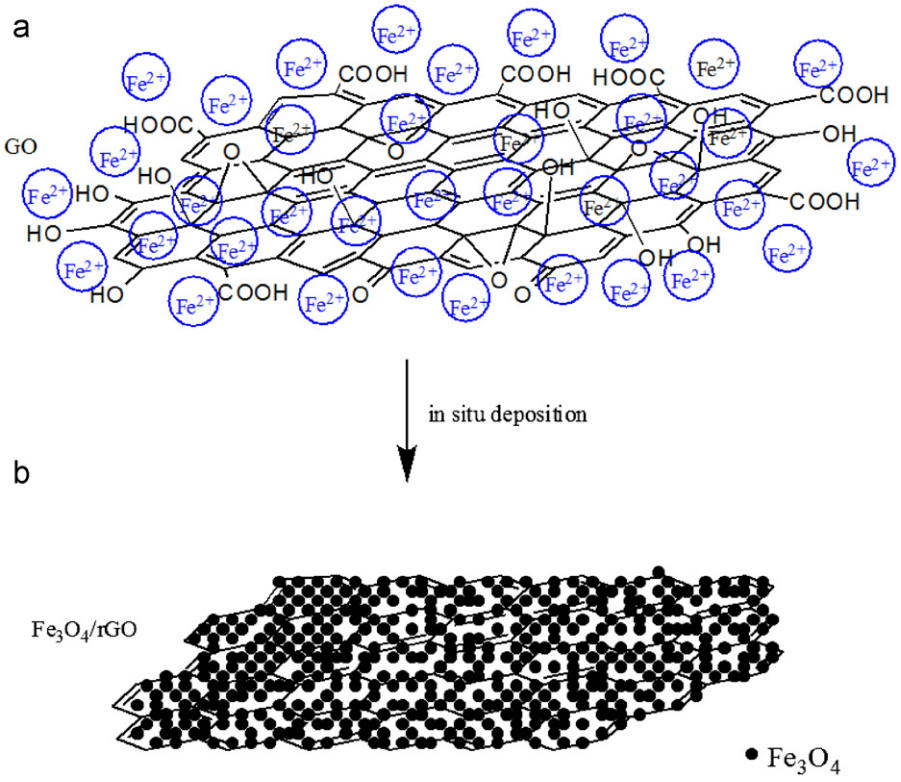

Fig. 4. Schematic illustration of the formation of Fe_3O_4/rGO nanocomposite via a one-step in situ chemical deposition method.

hybridization between GO and Fe^{2+} to form the Fe_3O_4/rGO nanocomposite is shown in Fig. 4, and is similar to our previously reported work [32]. The Fe^{2+} ions are first coordinated onto the surface of the GO sheets (Fig. 4a). The GO acts as an oxidizing agent (Eq. (1)), effectively increasing the oxidation state of the Fe ions from Fe^{2+} to Fe^{3+}. This is followed by the reaction of the Fe^{3+} ions, in an alkaline condition, into Fe_3O_4 nanoparticles (Eq. (2)) on the surface of the rGO. The formation of Fe_3O_4 could also occur using the OH^- groups attached to the GO surface (Eq. (3)). During the redox reaction, the polar oxygenated functional groups on the GO sheets serve as the anchoring sites for the Fe_3O_4 nanoparticles, consequently preventing serious agglomeration of the magnetic nanoparticles (Fig. 4b).

$$2Fe^{2+} + GO \rightarrow 2Fe^{3+} + rGO \quad (1)$$

$$Fe^{2+} + 2Fe^{3+} + 8OH^- \rightarrow Fe_3O_4 + 4H_2O \quad (2)$$

$$3Fe^{2} + GO(8OH^-) \rightarrow Fe_3O_4 + 4H_2O + rGO \quad (3)$$

4. Conclusion

Fe_3O_4 nanoparticles decorated on rGO sheets were successfully synthesized using a simple, easy, and low-cost in situ chemical synthesis approach in an alkaline condition. Increasing the weight ratio of Fe^{2+} to GO increases the Fe_3O_4 particle size on the GO sheets and the magnetic strength of the nanocomposites. The Fe_3O_4/rGO nanocomposites were dispersible in polar solvents for all the prepared weight ratios and were magnetic, and thus they are a promising material for multifunctional applications.

Acknowledgements

This work was supported by the Exploratory Research Grant Scheme (ER016–2011A), the Fundamental Research Grant Scheme (UKM-FST-07-FRGS0233–2010), the High Impact Research Grant of the University of Malaya (UM.C/625/1/HIR/030) and the High Impact Research Grant from the Ministry of Higher Education of Malaysia (UM.C/625/1/HIR/MOHE/05).

References

[1] V. Singh, D. Joung, L. Zhai, S. Das, S.I. Khondaker, S. Seal, Graphene based materials: past, present and future, Progress in Material Science 56 (2011) 1178–1271.
[2] X. Huang, X. Qi, F. Boey, H. Zhang, Graphene-based composites, Chemical Society Reviews 41 (2011) 666–686.
[3] X.M. Chen, Y.Q. Jiang, Y.R. Wang, X. Chen, Graphene and graphene-based nanomaterials: the promising materials for bright future of electroanalytical chemistry, Analyst 136 (2011) 4631–4640.
[4] Y. Kong, D.L. Zhao, L.Z. Bai, Z.M. Shen, Easy synthesis and characterization of high quality graphene sheets produced from mesocarbon microbeads, Material Letters 65 (2011) 2739–2741.

[5] Q. Cheng, J. Tang, J. Ma, H. Zhang, N. Shinya, L.C. Qin, Graphene and nanostructured MnO_2 composite electrodes for supercapacitors, Carbon 49 (2011) 2917–2925.
[6] Q. Qu, S. Yang, X. Feng, 2D sandwich-like sheets of iron oxide grown on graphene as high energy anode material for supercapacitors, Advanced Materials 23 (46) (2011) 5578–5580.
[7] Y.R. Lee, M.S. Song, K.M. Lee, I.Y. Kim, S.J. Hwang, Synthesis and electrochemical characterization of reduced graphene oxide-manganese oxide nanocomposites, Journal of Electrochemical Science and Technology 2 (2011) 1–7.
[8] Z.S. Wu, G. Zhou, L.C. Yin, W. Ren, F. Li, H.M. Cheng, Graphene/metal oxide composite electrode materials for energy storage, Nano Energy 1 (2012) 107–131.
[9] D. Ghosh, S. Chandra, A. Chakraborty, S.K. Ghosh, P. Pramanik, A novel graphene oxide-para amino benzoic acid nanosheet as effective drug delivery system to treat drug resistant bacteria, International Journal of Pharmaceutical Science and Drug Research 2 (2010) 127–133.
[10] B. Li, H. Cao, G. Yin, Y. Lu, J. Yin, Cu_2O@reduced graphene oxide composite for removal of contaminants from water and supercapacitors, Journal of Material Chemistry 21 (2011) 10645–10648.
[11] K. Zhang, V. Dwivedi, C. Chi, J. Wu, Graphene oxide/ferric hydroxide composites for efficient arsenate removal from drinking water, Journal of Hazardous Material 182 (2010) 162–168.
[12] V. Chandra, J. Park, Y. Chun, J.W. Lee, I.C. Hwang, K.S. Kim, Water-dispersible magnetite-reduced graphene oxide composites for arsenic removal, American Chemical Society 4 (2010) 3979–3986.
[13] X. Liu, L. Pan, Q. Zha, T. Lv, G. Zhu, T. Chen, T. Lu, Z. Sun, C. Sun, UV-assisted photocatalytic synthesis of ZnO-reduced graphene oxide composites with enhanced photocatalytic activity in reduction of Cr(VI), Chemical Engineering Journal 183 (2012) 238–243.
[14] C.L. Sun, H.H. Lee, J.M. Yang, C.C. Wu, The simultaneous electrochemical detection of ascorbic acid, dopamine, and uric acid using graphene/size-selected Pt nanocomposites, Biosensors and Bioelectronics 26 (2011) 3450–3455.
[15] C.L. Sun, H.H. Lee, J.M. Ying, C.C. Wu, The simultaneous electrochemical detection of ascorbic acid, dopamine, and uric acid using graphene/size-selected Pt nanocomposites, Biosensors and Bioelectronics 26 (2011) 3450–3455.
[16] W. Lu, Y. Luo, G. Chang, X. Sun, Synthesis of functional SiO_2-coated graphene oxide nanosheets decorated with Ag nanoparticles for H_2O_2 and glucose detection, Biosensors and Bioelectronics 26 (2011) 4791–4797.
[17] Y. Fan, H.T. Lu, J.H. Liu, C.P. Yang, Q.S. Jing, Y.X. Zhang, X.K. Yang, K.J. Huang, Hydrothermal preparation and electrochemical sensing properties of TiO_2–graphene nanocomposite, Colloids and Surfaces B 83 (2010) 78–82.
[18] D.H. Kim, Y.S. Yun, H.J. Jin, Difference of dispersion behavior between graphene oxide and oxidized carbon nanotubes in polar organic solvents, Current Applied Physics 12 (2012) 637–642.
[19] D.R Dreyer, S. Park, C.W. Bielawsk, R.S. Ruoff, The chemistry of graphene oxide, Chemical Society Reviews 39 (2010) 228–240.
[20] J. Liu, H. Jeong, J. Liu, K. Lee, J.Y. Park, Y.H. Ahn, S. Lee, Reduction of functionalized graphite oxides by trioctylphosphine in non-polar organic solvents, Carbon 48 (2010) 2282–2289.
[21] V.K. Singh, M.K. Pantra, M. Manoth, G.S. Gowd, S.R. Vadera, N. Kumar, In situ synthesis of graphene oxide and its composites with iron oxide, New Carbon Materials 24 (2009) 147–152.
[22] Y. Zhan, F. Meng, X. Yang, X. Liu, Magnetite-graphene nanosheets (GNs)/poly(arylene ether nitrile) (PEN): fabrication and characterization of a multifunctional nanocomposite film, Colloids and Surfaces A 390 (1–3) (2011) 112–119.
[23] Y. Zhan, F. Meng, Y. Lei, R. Zhao, J. Zhong, X. Liu, One-pot solvothermal synthesis of sandwich-like graphene nanosheets/Fe_3O_4 hybrid material and its microwave electromagnetic properties, Materials Letters 65 (2011) 1737–1740.
[24] H. Wu, G. Gao, X. Zhou, Y. Zhang, S. Guo, Control on the formation of Fe_3O_4 nanoparticles on chemically reduced graphene oxide surfaces, CrystEngComm 14 (2) (2012) 499–504.
[25] F. He, J. Fan, D. Ma, L. Zhang, C. Leung, H.L. Chan, The attachment of Fe_3O_4 nanoparticles to graphene oxide by covalent bonding, Carbon 48 (2010) 3139–3144.
[26] D. Lu, Y. Zhang, L Wang, S. Lin, C. Wang, X. Chen, Sensitive detection of acetaminophen based on Fe_3O_4 nanoparticles-coated poly(diallyldimethylammonium chloride)-functionalized graphene nanocomposite film, Talanta 88 (2012) 181–186.
[27] H. He, C. Gao, Supraparamagnetic, conductive, and processable multifunctional graphene nanosheets coated with high-density Fe_3O_4 nanoparticles, Applied Materials and Interfaces 2 (2010) 3201–3210.
[28] H.N. Lim, N.M. Huang, S.S. Lim, I. Harrison, C.H. Chia, Fabrication and characterization of graphene hydrogel via hydrothermal approach as a scaffold for preliminary study of cell growth, International Journal of Nanomedicine 6 (2011) 1817–1823.
[29] Y. Xue, H. Chen, D. Yu, S. Wang, M. Yardeni, Q. Dai, M. Guo, Y. Liu, F. Lu, J. Qu, L. Dai, Oxidizing metal ions with graphene oxide: the in situ formation of magnetic nanoparticles on self-reduced graphene sheets for multifunctional applications, Chemical Communications 47 (2011) 11689–11691.
[30] H.N. Lim, N.M. Huang, C.H. Loo, Facile preparation of graphene-based chitosan films: enhanced thermal, mechanical and antibacterial properties, Journal of Non-Crystalline Solids 358 (2012) 525–530.
[31] X. Wang, H. Tian, Y. Yang, H. Wang, S. Wang, W. Zhang, Y. Liu, Reduced graphene oxide/CdS for efficiently photocatalystic degradation of methylene blue, Journal of Alloys and Compounds 524 (2012) 5–12.
[32] H.N. Lim, R. Nurzulaikha, I. Harrison, S.S. Lim, W.T. Tan, M.C. Yeo, M.A. Yarmo, Preparation and characterization of tin oxide, SnO_2 nanoparticles decorated graphene, Ceramics International 38 (2012) 4209–4216.